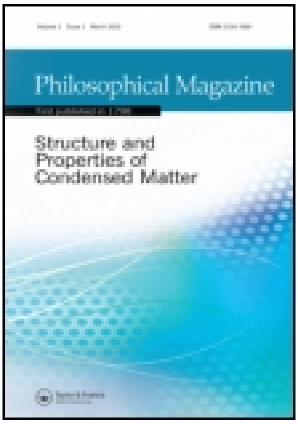


Philosophical Magazine
Publication details, including instructions for authors and subscription information:
http://www.tandfonline.com/loi/tphm20

# Prediction of effective stagnant thermal conductivities of porous materials at high temperature by the generalized self-consistent method

C.P. Jiang [a b] , F.L. Chen [a] , P. Yan [a] & F. Song [b]

[a] School of Aeronautic Science and Engineering, Beijing University of Aeronautics and Astronautics, Beijing 100191, China

[b] State Key Laboratory of Nonlinear Mechanics (LNM), Institute of Mechanics, Chinese Academy of Sciences, Beijing 100190, China

Version of record first published: 24 Feb 2012.

To cite this article: C.P. Jiang, F.L. Chen, P. Yan & F. Song (2012): Prediction of effective stagnant thermal conductivities of porous materials at high temperature by the generalized self-consistent method, Philosophical Magazine, 92:16, 2032-2047

To link to this article: http://dx.doi.org/10.1080/14786435.2012.661888

*Philosophical Magazine*
Vol. 92, No. 16, 1 June 2012, 2032–2047



# Prediction of effective stagnant thermal conductivities of porous materials at high temperature by the generalized self-consistent method

C.P. Jiang[ab]*, F.L. Chen[a], P. Yan[a] and F. Song[b]

[a]*School of Aeronautic Science and Engineering, Beijing University of Aeronautics and Astronautics, Beijing 100191, China;* [b]*State Key Laboratory of Nonlinear Mechanics (LNM), Institute of Mechanics, Chinese Academy of Sciences, Beijing 100190, China*

(*Received 13 July 2011; final version received 25 January 2012*)

The generalized self-consistent method is developed to deal with porous materials at high temperature, accounting for thermal radiation. An exact closed form formula of the local effective thermal conductivity is obtained by solving Laplace's equation, and a good approximate formula with uncoupled conductive and radiative effects is given. A comparison with available experimental data and theoretical predictions demonstrates the accuracy and efficiency of the present formula. Numerical examples provide a better understanding of interesting interaction phenomena of pores in heat transfer. It is found that the local effective thermal conductivity divides into two parts. One, attributed to conduction, is independent of pore radius for a fixed porosity and, furthermore, is independent of temperature (actually, it is approximately independent of the temperature) if it is non-dimensionalized by the thermal conductivity of the matrix. The other is due to thermal radiation in pores and strongly depends on the temperature and pore radius. The radiation effect can not be neglected at high temperature and in the case of relatively large pores.

**Keywords:** porous material; effective thermal conductivity; generalized self-consistent method; thermal radiation; high temperature



## 1. Introduction

Porous materials possess superior mechanical and thermal performances, such as light weight, high specific strength, high specific stiffness, high toughness, high energy absorption and excellent thermal insulation, and have been widely used in aeronautics, astronautics, atomic energy, transportation industries, etc. [1,2].

Heat transport in porous materials, which has aroused the concern of many researchers [3–9], occurs via three ways: (i) heat conduction in solid and gas; (ii) thermal radiation in pores; (iii) convection of gas in pores. These ways are always coupled with each other. To simplify the problem, it is necessary to ignore some

*Corresponding author. Email: jiangchiping@buaa.edu.cn

ISSN 1478–6435 print/ISSN 1478–6443 online

http://dx.doi.org/10.1080/14786435.2012.661888
http://www.tandfonline.com

minor factors. In this paper, the following two assumptions are employed:

(1) When the pores are almost, or entirely, disconnected the convection in pores is negligible.
(2) The gas is assumed to be transparent, and the pore surface to be a diffuse-gray surface when the thermal radiation effect is considered.

For materials with small pores at low temperature, the radiative effect is negligible for most practical purposes. However, with the elevation of temperature and the increase of the pore size, the radiative contribution becomes significant. Many investigations have been carried out on the thermal properties of porous materials in the case of pure conduction, whereas studies accounting for the radiative effect are still limited. Among the small number of studies, Chiew and Glandt [4] addressed the problem of effective thermal conductivities of porous and composite materials, accounting for the effect of radiation. They obtained an exact solution of the temperature and temperature gradient fields of the dilute scheme by solving Laplace's equation, and the exact solution was used to calculate effective thermal conductivities integrated with Maxwell's result. Liang and Qu [5] dealt with the effective thermal conductivity of gas–solid composite materials at high temperature, and they assumed that the pores were arranged periodically, temperature linearly distributed along the heat flux and that the pore surface was black. Liu and Zhang [7] presented a homogenization-based multi-scale method for the thermal conductivity of porous materials with radiation, and they took the temperature distribution in the case of the pure conduction as the approximation of the real temperature field. Wang and Pan [8] developed a random generation-growth method to reproduce the microstructures of open-cell foam materials via computer modeling, and they used the high-efficiency lattice Boltzmann method to solve the energy transport equations. Zhao et al. [9] developed an explicit analytical method to describe the thermal radiation process in open-cell metal foams with idealized cellular morphologies. Related to the topic of thermal radiation in porous materials, Liu [10] established a mathematical relationship between the specific surface area and the porosity and pore diameter, and then proposed a method for calculating the specific surface area of porous metal foams.

The generalized self-consistent method [11–20] is a sophisticated micromechanics method, which is of mathematical rigor in its formulation and physical realism [18]. The method can provide compact formulae and reasonable results, and has been widely used to predict the mechanical [11,12,14–16] and thermal [13,17,19,20] properties (pure conduction) of composite materials. However, to the best of our knowledge, the method has not been extended to predict the effective thermal conductivity of porous materials accounting for the radiative contribution in pores. The purpose of the present work is to develop such a micromechanics method to acquire a better understanding of interesting interaction phenomena of pores in heat transfer at high temperature.

This paper is organized as follows. In Section 2, the basic formulae of the effective thermal conductivity are derived by using the generalized self-consistent method, and the thermal fluxes in the representative volume element are divided into conductive and radiative fluxes. Section 3 calculates the exact temperature fields in the generalized self-consistent model. Section 4 deals with the average radiative flux

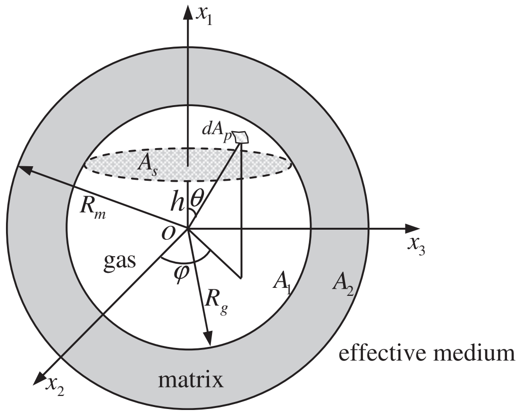


Figure 1. A schematic diagram of the generalized self-consistent model.



on the diffuse-gray surface of the pore by using the net-radiation method. In Section 5, a closed form formula of the local effective thermal conductivity is obtained, and a concise approximate formula with high accuracy is given, where the conductive and radiative effects are uncoupled. In Section 6, numerical examples are presented, and a comparison is made with available results. Many interesting phenomena, in which the porosity and pore radius influence the conduction and radiation in different ways, are revealed and discussed.

## 2. Model and basic formula

A schematic diagram of the generalized self-consistent model is shown in Figure 1. The representative volume element consists of a spherical matrix shell and a concentric gas pore, which is embedded in an infinite effective medium with the as-yet-unknown effective thermal conductivity. The porosity of the representative volume element is equal to that of the whole porous material, so that

$$\lambda = \frac{R_g^3}{R_m^3}, \tag{1}$$

where $\lambda$, $R_g$ and $R_m$ are the porosity, the pore radius and the external radius of the representative volume element. At steady state, the heat transfer in each phase of the generalized self-consistent model can be described by

$$\nabla \cdot (k_i \nabla T_i) = 0 \quad i = g, m, e, \tag{2}$$

where $k$ is the thermal conductivity, $T$ is the absolute temperature and the subscripts $g$, $m$ and $e$ refer to the gas in the pore, the spherical matrix shell and the outside effective medium, respectively.

According to the generalized self-consistent method, the effective thermal conductivity of isotropic porous materials, $k_e$, can be determined by the representative volume element:

$$k_e = -\frac{\langle q \rangle}{\langle H \rangle}, \tag{3}$$

where $q$ and $H$ are the heat flux and temperature gradient, respectively. The sign $\langle \bullet \rangle$ denotes averaging over the representative volume element:

$$\begin{cases} \langle q \rangle = \langle q \rangle_g \lambda + \langle q \rangle_m (1 - \lambda) \\ \langle H \rangle = \langle H \rangle_g \lambda + \langle H \rangle_m (1 - \lambda) \end{cases}, \tag{4}$$

where

$$\begin{cases} \langle \bullet \rangle_g = \dfrac{1}{V_g} \displaystyle\int_{V_g} \bullet \, \mathrm{d}V \\ \langle \bullet \rangle_m = \dfrac{1}{V_m} \displaystyle\int_{V_m} \bullet \, \mathrm{d}V \end{cases} \tag{5}$$

and $V_g$ and $V_m$ are the volumes of the pore and matrix shell in the representative volume element, respectively.

The remaining work is to determine the average heat flux $\langle q \rangle$ and temperature gradient $\langle H \rangle$ in the representative volume element. As pointed out in the introduction, for materials with almost or entirely disconnected pores, the convection in pores is negligible and the total average heat flux in the representative volume element can be divided into two parts: one is attributed to conduction in solid and gas and the other is due to thermal radiation in pores, so that

$$\langle q \rangle = \langle q \rangle^c + \langle q \rangle^r, \tag{6}$$

where

$$\begin{cases} \langle q \rangle^c = \lambda \langle q \rangle_g^c + (1 + \lambda) \langle q \rangle_m \\ \langle q \rangle^r = \lambda \langle q \rangle_g^r, \end{cases} \tag{7}$$

and the superscript $c$ and $r$ refer to conduction and radiation, respectively. $\langle q \rangle^c$ and $\langle q \rangle^r$ will be derived in the following sections.

## 3. Exact temperature fields in the generalized self-consistent model

The calculation of the average heat flux $\langle q \rangle$ and the temperature gradient $\langle H \rangle$ requires the temperature fields in the pore, matrix shell and effective medium in the generalized self-consistent model. Let the far-field uniform temperature gradient be $H_0$ along the $x_1$ direction (Figure 1). The general form of the solutions in spherical coordinates for an axially symmetric case [4] is

$$T(x) = \sum_{j=0}^{\infty} P_j(\cos\theta)(A_j r^j + B_j r^{-(j+1)}), \tag{8}$$

where $P_j$ is the Legendre polynomial of degree $j$ and $A_{gj}$, $B_{gj}$, $A_{mj}$, $B_{mj}$, $A_{ej}$ and $B_{ej}$ are real constants.

To obtain these real constants, the following boundary conditions are used: (i) $T_g$ bounded at $r=0$; (ii) uniform gradient at the far-field, i.e. $T_e \to H_0 r\cos\theta$ as $r \to \infty$; (iii) continuities of temperatures at the surfaces of the pore and matrix shell, i.e. $T_g = T_m$ at $r = R_g$, $T_m = T_e$ at $r = R_m$; (iv) continuities of the normal fluxes at the surfaces of the pore and matrix shell, including the radiation contribution at the pore surface.

The view factor [21] from an arbitrary infinitesimal area $\mathrm{d}A_j$ to another $\mathrm{d}A_p$ is

$$\mathrm{d}F_{dA_j-dA_p} = \frac{1}{4\pi R_g^2}\mathrm{d}A_p. \tag{9}$$

When the pore surface is assumed to be a diffuse-gray surface, the radiative heat flux $q_p^r$ at an infinitesimal area $\mathrm{d}A_p$ can be expressed as

$$q_p^r = q_p^{out} - q_p^{in}, \tag{10}$$

where $q_p^{out}$ and $q_p^{in}$ denote the emission flux and incidence flux, respectively. The emissive flux $q_p^{out}$ can be written as

$$q_p^{out} = \varepsilon\sigma T^4_{(\theta_p,\varphi_p)} + \rho q_p^{in} = \varepsilon\sigma T^4_{(\theta_p,\varphi_p)} + (1-\varepsilon)q_p^{in}, \tag{11}$$

where $\varepsilon$, $\rho$ and $\sigma$ are the emissivity, reflectivity and Stefan–Boltzmann constant, respectively, and $T_{(\theta,\varphi)}$ denotes the temperature on the boundary at point $(\theta,\varphi)$. The relation $\rho = 1-\varepsilon$ has been considered in Equation (11) for the diffuse-gray surface. The incidence flux $q_p^{in}$ can be given as

$$q_p^{in}\mathrm{d}A_p = \int_{A_1} q_j^{out}\mathrm{d}A_j\mathrm{d}F_{\mathrm{d}A_j-\mathrm{d}A_p}. \tag{12}$$

According to the reciprocity of the view factor, Equation (12) can be rewritten as

$$q_p^{in} = \int_{A_1} q_j^{out}\mathrm{d}F_{\mathrm{d}A_p-\mathrm{d}A_j}. \tag{13}$$

Substituting Equation (13) into Equation (11), one obtains

$$\begin{aligned} q_p^{out} &= \varepsilon\sigma T^4_{(\theta_p,\varphi_p)} + (1-\varepsilon)\int_{A_1} q_j^{out}\mathrm{d}F_{\mathrm{d}A_p-\mathrm{d}A_j} \\ &= \varepsilon\sigma T^4_{(\theta_p,\varphi_p)} + \frac{1-\varepsilon}{4\pi R_g^2}\int_{A_g} q_j^{out}\,\mathrm{d}A_j. \end{aligned} \tag{14}$$

The solution of Equation (14) can be assumed to be

$$q_p^{out} = f_{(\theta_p,\varphi_p)} + C, \tag{15}$$

where $f_{(\theta_p,\varphi_p)}$ is a function of the coordinates $(\theta_p,\varphi_p)$ and $C$ is a real constant. Substituting Equation (15) into Equation (14), one obtains

$$\begin{aligned} f_{(\theta_p,\varphi_p)} &= \varepsilon\sigma T^4_{(\theta_p,\varphi_p)} + \frac{1-\varepsilon}{4\pi R_g^2}\int_{A_g}(f_{(\theta_j,\varphi_j)} + C)\mathrm{d}A_j - C \\ &= \varepsilon\sigma T^4_{(\theta_p,\varphi_p)} - C\varepsilon + \frac{1-\varepsilon}{4\pi R_g^2}\int_{A_g} f_{(\theta_j,\varphi_j)}\mathrm{d}A_j. \end{aligned} \tag{16}$$

Observing Equation (16), one obtains

$$\begin{cases} f_{(\theta_p,\varphi_p)} = \varepsilon\sigma T^4_{(\theta_p,\varphi_p)} \\ C = \dfrac{1-\varepsilon}{4\pi\varepsilon R_g^2}\displaystyle\int_{A_g} f_{(\theta_j,\varphi_j)}\mathrm{d}A_j. \end{cases} \tag{17}$$

Substituting $f_{(\theta_j,\varphi_j)}$ into $C$, one obtains

$$C = \frac{(1-\varepsilon)\sigma}{4\pi R_g^2}\int_{A_g} T^4_{(\theta_j,\varphi_j)}\mathrm{d}A_j. \tag{18}$$

The emission flux $q_p^{out}$ can be rewritten as

$$q_p^{out} = \varepsilon\sigma T^4_{(\theta_p,\varphi_p)} + \frac{(1-\varepsilon)\sigma}{4\pi R_g^2}\int_{A_g} T^4_{(\theta_j,\varphi_j)}\mathrm{d}A_j. \tag{19}$$

Substituting Equations (19) and (11) into Equation (10), the radiative heat flux, $q_p^r$, on the surface at an arbitrary point is given as

$$\begin{aligned} q_p^r &= q_p^{out} - \frac{1}{1-\varepsilon}\left(q_p^{out} - \varepsilon\sigma T^4_{(\theta_p,\varphi_p)}\right) \\ &= \frac{\varepsilon}{1-\varepsilon}\left(\sigma T^4_{(\theta_p,\varphi_p)} - \varepsilon\sigma T^4_{(\theta_p,\varphi_p)} - \frac{(1-\varepsilon)\sigma}{4\pi R_g^2}\int_{A_g} T^4_{(\theta_j,\varphi_j)}\mathrm{d}A_j\right) \\ &= \frac{\varepsilon\sigma}{4\pi R_1^2}\int_{A_1}\left(T^4_{(\theta_p,\varphi_p)} - T^4_{(\theta_j,\varphi_j)}\right)\mathrm{d}A_j \\ &= \frac{\varepsilon\sigma}{2}\int_{\theta_{j=0}}^{\pi}\left(T^4_{(\theta_p,\varphi_p)} - T^4_{(\theta_j,\varphi_j)}\right)\sin\theta_j\mathrm{d}\theta_j \end{aligned} \tag{20}$$

If we linearize $T^4$ about an average temperature for the sphere, $T_0$, Equation (20) can be rewritten as

$$q_p^r = 2\varepsilon\sigma T_0^3\int_{\theta_{j=0}}^{\pi}\left(T_{(\theta_p,\varphi_p)} - T_{(\theta_j,\varphi_j)}\right)\sin\theta_j\mathrm{d}\theta_j. \tag{21}$$

Hence, the continuity of the flux at the pore surfaces is

$$k_g\frac{\partial T_g}{\partial r}\bigg|_{r=R_g} - k_m\frac{\partial T_m}{\partial r}\bigg|_{r=R_g} = 2\varepsilon\sigma T_0^3\int_{\theta_{j=0}}^{\pi}\left(T_{(\theta_p,\varphi_p)} - T_{(\theta_j,\varphi_j)}\right)\sin\theta_j\mathrm{d}\theta_j. \tag{22}$$

The resulting temperature fields are

$$\begin{cases} T_g = A_g r\cos\theta & r \le R_g \\ T_m = \left(A_m r + \dfrac{B_m}{r^2}\right)\cos\theta & R_g < r \le R_m \\ T_e = \left(H_0 r + \dfrac{B_e}{r^2}\right)\cos\theta & r > R_m \end{cases} \tag{23}$$

where

$$
\begin{cases}
A_g = 9H_0 k_m k_e R_m^3/Z \\
A_m = 3H_0 k_e R_m^3 (k_g + 2k_m + 4\varepsilon\sigma R_g T_0^3)/Z \\
B_m = -3H_0 k_e R_g^3 R_m^3 \left(k_g - k_m + 4\varepsilon\sigma R_g T_0^3\right)/Z \\
B_e = -\Big[H_0(k_g - K_m)(2k_m + k_e)R_g^3 R_m^3 - H_0(k_e - k_m)(2k_m + k_g)R_m^6 \\
\qquad + 4\varepsilon\sigma H_0 R_g^4 R_m^3 T_0^3 (2k_m + k_e) + 4\varepsilon\sigma H_0 R_g R_m^6 T_0^3 (k_m - k_e)\Big]/Z
\end{cases}
\tag{24}
$$

and

$$
\begin{aligned}
Z = {} & 2(k_e - K_m)(k_m - k_g)R_g^3 + (2k_e + k_m)(2k_m + k_g)R_m^3 \\
& + 4\varepsilon\sigma R_g T_0^3 \Big[2(k_m - k_e)R_g^3 + (2k_e + k_m)R_m^3\Big]
\end{aligned}
\tag{25}
$$

Letting $k_e = k_m$, the solution given by Equation (23) degenerates into the exact result of the existing dilute scheme [4]. It should be pointed out that the solution given by Equation (23) can be used to study the temperature and heat flux fields in a composite with hollow spherical inclusions at high temperature, which will be left for readers. In the following, the solution given by Equation (23) will be used to estimate the effective thermal conductivity.

## 4. Average radiative heat flux

Referring to Figure 1, the interior boundary $A_1$ divides into two parts, upside and underside by $A_s$ at $x_1 = h$. Because there is no internal heat source in a closed region made by $A^{up}$ and $A_s$, the heat quantity from $A^{up}$ into the gas phase is equal to the heat quantity $Q_{A_s}^r$ across $A_s$. Thus, $Q_{A_s}^r$ can be described as

$$
Q_{A_s}^r = \int_{A^{up}} q_p^r \, \mathrm{d}A_p = \int_{\theta_p=0}^{\beta} \int_{\varphi_p}^{2\pi} q_p^r R_g^2 \sin\theta_p \, \mathrm{d}\varphi_p \, \mathrm{d}\theta_p, \tag{26}
$$

where $\beta = \arccos(h/R_g)$. Then the average radiative flux within the pore can be written as

$$
\langle q \rangle_g^r = \frac{1}{V_g} \int_{V_g} q^r \mathrm{d}V = \frac{3}{4\pi R_g^3} \int_{R_g}^{-R_g} Q_{A_s}^r \mathrm{d}h. \tag{27}
$$

Substituting Equations (20) and (26) into Equation (27), one obtains

$$
\langle q \rangle_g^r = -4\sigma\varepsilon A_g R_g T_0^3. \tag{28}
$$

## 5. Effective thermal conductivity

### 5.1. *Exact solution by the generalized self-consistent method*

From Equations (23) and (5), the average temperature gradients in the pore and matrix can be written as

$$
\begin{cases}
\langle H \rangle_g^{x_1} = A_g \quad \langle H \rangle_g^{x_2} = 0 \quad \langle H \rangle_g^{x_3} = 0 \\
\langle H \rangle_m^{x_1} = A_m \quad \langle H \rangle_m^{x_2} = 0 \quad \langle H \rangle_m^{x_3} = 0
\end{cases}. \tag{29}
$$

From Fourier's law, the average temperature gradient and average heat flux in the pore and matrix have following relations:

$$\langle q\rangle_g^c = -k_g\langle H\rangle_g, \quad \langle q\rangle_m = -k_m\langle H\rangle_m. \tag{30}$$

Thus, the average temperature gradients and average heat fluxes along the $x_1$-direction induced by pure conduction are obtained as

$$\begin{cases} \langle H\rangle_g = A_g; & \langle H\rangle_m = A_m \\ \langle q\rangle_g^c = -k_g A_g; & \langle q\rangle_m = -k_m A_m \end{cases} \tag{31}$$

Substituting Equations (28), (31) and (6) into Equation (3), one obtains the effective thermal conductivity of the porous materials

$$\begin{aligned} k_e &= -\frac{\left[\lambda\langle q\rangle_g^c + (1-\lambda)\langle q\rangle_m\right] + \lambda\langle q\rangle_g^r}{\lambda\langle H\rangle_g + (1-\lambda)\langle H\rangle_m} \\ &= \frac{\lambda k_g + (1-\lambda)k_m\frac{A_m}{A_g} + 4\lambda\varepsilon\sigma R_g T_0^3}{\lambda + (1-\lambda)\frac{A_m}{A_g}} \end{aligned} \tag{32}$$

From Equation (24), one obtains

$$\frac{A_m}{A_g} = \frac{1}{3k_m}(k_g + 2k_m + 4\varepsilon\sigma R_g T_0^3). \tag{33}$$

It is very interesting to observe that the effective thermal conductivity, Equation (32), can be proved consistent with Chiew and Glandt's formula [4], which is derived by the dilute scheme integrated with Maxwell's result. The present work and their work verify and complement each other. However, the emphasis of the present work is not on the novel model and method, but a better scientific understanding of interesting interaction phenomena of pores on heat transfer (especially, a very different dependence of the conductive and radiative effects on microstructural parameters). To do this, an approximate solution with uncoupled conductive and radiative effects is highly desirable.

### 5.2. *Approximate solution with uncoupled conductive and radiative effects*

The far-field condition of the generalized self-consistent model is the uniform temperature gradient $H_0$. The calculation of the effective thermal conductivity required the average temperature gradient $\langle H\rangle$. The fact implies that one may obtain a good approximate solution by leaving out the disturbance of the local temperature gradient field induced by radiation. Letting the temperature gradient field with radiative effect be approximately equal to that by pure conduction, then the continuity of the flux at the pore surfaces (Equation (22)) is reduced to

$$k_g\frac{\partial T_g}{\partial r}\bigg|_{r=R_g} = k_m\frac{\partial T_m}{\partial r}\bigg|_{r=R_g}, \tag{34}$$

and $\frac{A_m}{A_g}$ in Equation (32) becomes

$$\frac{A_m}{A_g} = \frac{1}{3}\left(2 + \frac{k_e}{k_m}\right). \tag{35}$$

The effective thermal conductivity (Equation (32)) is decoupled:

$$k_e = k_e^c + k_e^r, \tag{36}$$

where $k_e^c$ is the effective thermal conductivity by pure conduction and $k_e^r$ represents the radiative contribution:

$$k_e^c = \frac{k_g + 2k_m + 2\lambda(k_g - k_m)}{k_g + 2k_m - \lambda(k_g - k_m)} k_m, \tag{37}$$

$$k_e^r = \frac{12\lambda\sigma\varepsilon k_m R_g T_0^3}{3\lambda k_m + (1-\lambda)(2k_m + k_g)}. \tag{38}$$

Equation (37) is in agreement with classical formula for pure conduction [13]. When the radiative effect is absent, i.e. emissivity $\varepsilon = 0$, Equation (32) also degenerates into Equation (37).

### 5.3. *Accuracy of the approximate solution*

Now examine the accuracy of the approximate solution, Equation (36). In the following numerical example of porous alumina, the data for the thermal conductivities ($k_m$ and $k_g$) of the alumina and the gas in pores at different temperatures are taken from [22] and are listed in Table 1.

A comparison between the exact solution (Equation (32)) and approximate solution (Equation (36)) of the effective thermal conductivity is listed in Table 2, where the emissivity $\varepsilon = 0.5$, $R_g = 3\,\text{mm}$, $k_e$ and $\lambda$ are the effective thermal conductivity and the porosity, respectively, and error $= (k_e^{Eq(36)} - k_e^{Eq(32)})/k_e^{Eq(32)} \times 100\%$. Table 2 shows that Equation (36) with uncoupled conductive and radiative effects is a good approximate formula and will be used to study the interesting interaction phenomena of pores in heat transfer in the next section.

## 6. Results and discussion

A black pore surface, i.e. the emissivity $\varepsilon = 1$, was assumed by some researchers [5,7]. For convenience of comparison and discussion, such an assumption is also adopted in the following numerical computations.

Table 1. Thermal conductivities ($k_m$ and $k_g$) of the alumina and the gas in pores at different temperatures.

| Temperature (K) | 473 | 673 | 873 | 1073 |
|---|---|---|---|---|
| $k_m$ (W m$^{-1}$ K$^{-1}$) | 21.16 | 12.54 | 8.36 | 6.79 |
| $k_g$ (W m$^{-1}$ K$^{-1}$) | 0.03873 | 0.05091 | 0.06153 | 0.07178 |

Table 2. A comparison between the exact solution (Equation (32)) and approximate solution (Equation (36)) of the effective thermal conductivity, where the emissivity $\varepsilon = 0.5$, $R_g = 3$ mm.

| | | $k_e$ (W m$^{-1}$ K$^{-1}$) | | |
|---|---|---|---|---|
| $T_0$ (K) | $\lambda$ | Equation (32) | Equation (36) | Error (%) |
| 473 | 0.3 | 12.9181 | 12.9138 | −0.0330 |
| | 0.5 | 8.5178 | 8.5135 | −0.0505 |
| | 0.8 | 3.0915 | 3.0893 | −0.0710 |
| 673 | 0.3 | 7.7117 | 7.6995 | −0.1574 |
| | 0.5 | 5.1270 | 5.1148 | −0.2389 |
| | 0.8 | 1.9333 | 1.9270 | −0.3239 |
| 873 | 0.3 | 5.2341 | 5.2084 | −0.4910 |
| | 0.5 | 3.5499 | 3.5238 | −0.7326 |
| | 0.8 | 1.4580 | 1.4447 | −0.9150 |
| 1073 | 0.3 | 4.3788 | 4.3335 | −1.0340 |
| | 0.5 | 3.0652 | 3.0192 | −1.5011 |
| | 0.8 | 1.4195 | 1.3958 | −1.6713 |

### 6.1. *Comparison with experimental data and other theoretical results*

First of all, a comparison with available experimental data and theoretical predictions is made to demonstrate the accuracy and efficiency of the present formula.

Francl and Kingery [22] investigated the effective thermal conductivity of porous alumina materials by an experimental approach. Their specimens are one-inch cubes with uniformly distributed pores of the diameter 0.31 mm but different porosities, and their data of the thermal conductivities of the alumina and the gas in pores in different temperatures are listed in Table 1. By using the present exact and approximate formulae, Chiew and Glandt's formula [4], Francl and Kingery's experimental data [22] and Liang and Qu's theoretical predictions [5], the variations of the thermal conductivity with the porosity are shown in Figure 2a at a temperature of 673 K and in Figure 2b at a temperature of 1073 K. Liang and Qu [5] adopted an assumption that pores were periodically distributed and the temperature linearly distributed in a unit cell.

From Figure 2, it can be seen that the present exact and approximate formulae, Chiew and Glandt's formulae [4] provide almost the same results. They are not distinguishable in the figure because the maximum relative error is less than 0.18%.

From Figure 2b, it can be seen that the present predictions are in good agreement with the experimental data at the higher temperature of 1073 K. From Figure 2a, a deviation of about 10% between the present predictions and the experimental data is observed at the moderate temperature of 673 K. In the following, the reason for this deviation will be discussed further.

Agapiou and DeVries [23] reported that the temperature has little influence on the dimensionless or relative thermal conductivity, $k_e/k_m$, where $k_e$ and $k_m$ are the thermal conductivities of a porous material and its corresponding fully dense material, respectively. The radiative effect is proportional to the fourth power of

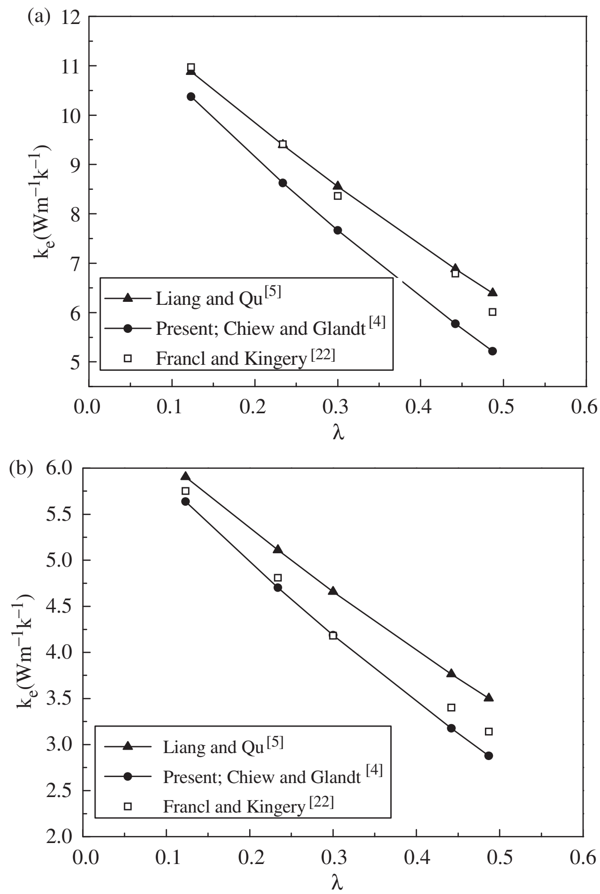


Figure 2. Variations of the effective thermal conductivity with the porosity: (a) at 673 K; (b) at 1073 K.



absolute temperature. At low and moderate temperatures, the radiative effect can be neglected and the effective thermal conductivity is given by Equation (37). Furthermore, if the thermal conductivity of the gas phase is very small compared with that of the solid phase, i.e. $\frac{k_1}{k_2} \approx 0$, Equation (37) is reduced to

$$\frac{k_e^c}{k_m} = 1 - \frac{3\lambda}{2+\lambda}. \tag{39}$$

By using Equation (39), the variations of the dimensionless thermal conductivity $k_e^c/k_m$ with the porosity were calculated and are plotted in Figure 3. For comparison, three sets of experimental data for an $Al_2O_3$ material with isometric pores [22] a 304L stainless steel material with irregular pores [23] and an $Al_2O_3$ material with irregular pores [24] are also plotted in Figure 3. It can be seen that the present predictions fall in the neighborhood of experimental statistical average values. It is worth noting that for the porous alumina materials in last example, the radiative effect at $T_0 = 673$ K is

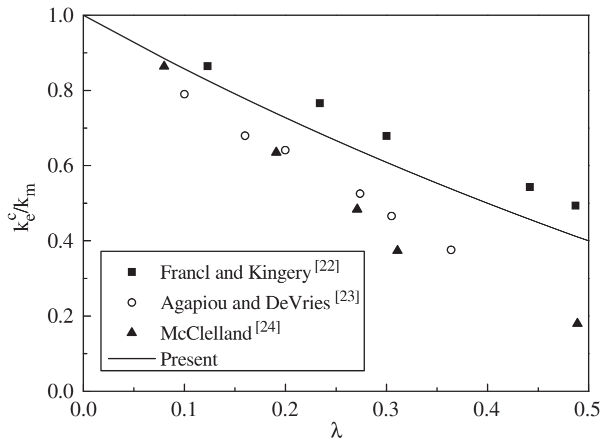


Figure 3. Comparisons of dimensionless thermal conductivity, $k_e^c/k_m$, with experimental data.

negligible, so Equation (39) can replace Equation (37) The deviation between the present predictions and the experimental data in Figure 2a is within experimental error. It can be seen that the deviation between experimental data is still large, and further experimental investigations are needed.

### 6.2. *Influence of the porosity on the effective thermal conductivity*

From Sections 5.3 and 6.1, it is concluded that the present approximate formula (Equations (36)–(38)) not only has good engineering accuracy, but also has the advantage that conductive and radiative effects are decoupled, i.e. the total effective thermal conductivity $k_e$ can be divided to two parts: $k_e^c$ corresponding to pure conduction and $k_e^r$ corresponding to the radiation in pores. In order to more clearly observe their respective contribution, consider the corresponding dimensionless quantities, $k_e^c/k_e$ and $k_e^r/k_e$. The variations of $k_e^c/k_e$ and $k_e^r/k_e$ with porosity for a fixed pore radius $R_g = 10\,\text{mm}$ and at several temperatures are plotted in Figure 4a and b, respectively. From Figure 4, contrary laws are observed: $k_e^c/k_e$ decreases with an increase of the porosity, whereas $k_e^r/k_e$ increases with an increase of the porosity. At the same time, it is also observed that the temperature has an important influence on the total effective thermal conductivity. The higher the temperature, the greater the radiative contribution. The present formula can help engineers to determine whether the radiative effect must be considered.

### 6.3. *Influence of the pore radius on the effective thermal conductivity*

It is well known that, in the case of the pure conduction, the effective thermal conductivity predicted by micromechanical methods is independent of the pore radius for a fixed porosity. However, when the radiative effect becomes significant, the total effective thermal conductivity strongly depends on it. The variations of

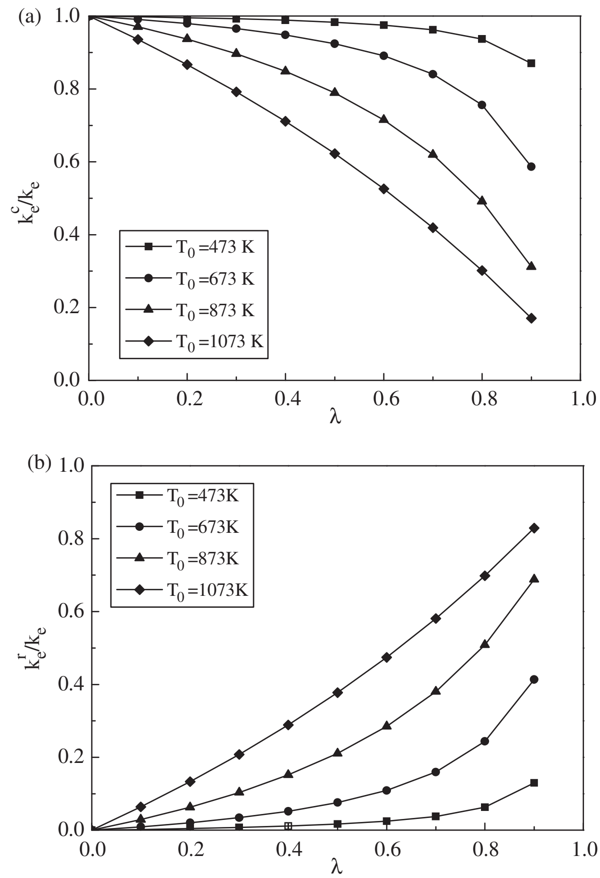


Figure 4. Variations of $k_e^c/k_e$ and $k_e^r/k_e$ with the porosity, $\lambda$, for the pore radius $R_g = 10$ mm at several temperatures.

$k_e^c/k_e$ and $k_e^r/k_e$ with the pore radius at several temperatures and for a fixed porosity $\lambda = 0.5$ are plotted in Figure 5a and b, respectively.

It can be seen that, at low temperature, the radiative contribution is small even though the pore radius goes up to 10 mm. However, at high temperature, the effective radiative thermal conductivity increases dramatically with the pore radius. It should be noted that the effective thermal conductivity by the pure conduction $k_e^c$ is independent of the pore radius for a fixed porosity, but $k_e^c/k_e$ depends on it.

## 7. Conclusions

(1) The exact solution of the temperature and temperature gradient fields in the generalized self-consistent model of porous materials accounting for coupling of conductive and radiative effects, derived by solving Laplace's equation

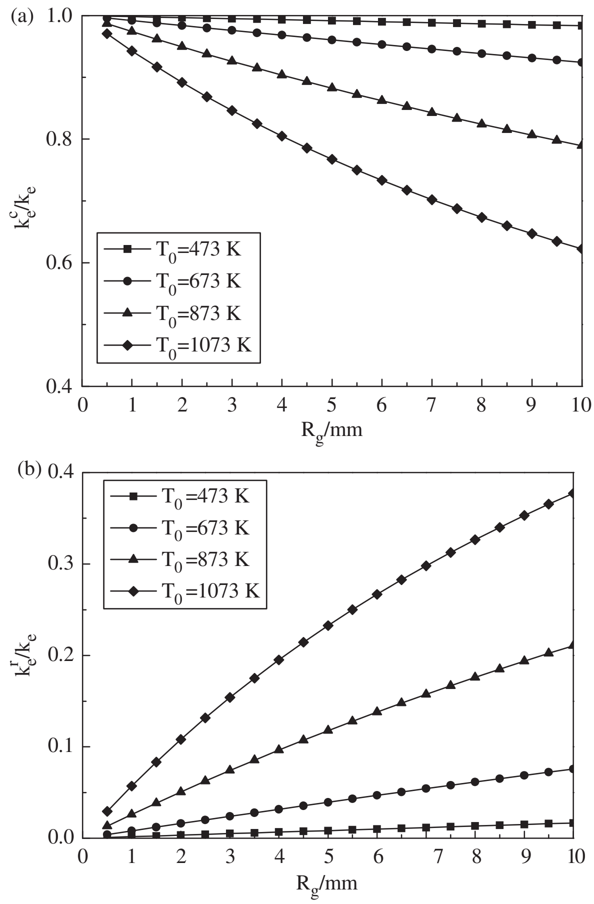


Figure 5. Variations of $k_e^c/k_e$ and $k_e^r/k_e$ with the pore radius for a fixed porosity $\lambda = 0.5$ and at several temperatures.



with the boundary conditions at infinity and at the interfaces between the pores and matrix phase and between the matrix and effective medium phases, can degenerate into the existing exact solution of the corresponding dilute scheme [4].

(2) The above exact solution can be used to study the temperature and heat flux fields in a composite with hollow spherical inclusions at high temperature. In this work, it has been used to develop the generalized self-consistent method to predict the effective thermal conductivity of porous materials accounting for the radiative effect, and a compact closed form formula is obtained. The present formula and that in [4] (by using the dilute scheme and Maxwell's result) verify and complement each other.

(3) A good approximate formula of the effective thermal conductivity with uncoupled conductive and radiative effects has been obtained. The uncoupled formula shows that the effective thermal conductivity of porous materials

consists of two parts, i.e. $k_e^c$ corresponding to the pure conduction and $k_e^r$ corresponding to the radiation in pores. $k_e^c$ is independent of the pore radius for a fixed porosity and $k_e^c/k_m$ is (actually approximately) independent of temperature, where $k_m$ is the thermal conductivities of the matrix. However, $k_e^r$ strongly depends on the pore radius and temperature. $k_e^r$ can not be neglected at high temperature and in the case of relative large pores.

The present work leads to a much better understanding of the interesting interacting phenomena of the conduction and radiation with the microstructure in porous materials and can help engineers to estimate the effective thermal conductivity of porous materials at high temperature and determine whether the radiative effect must be considered.



**Nomenclature**

| | |
|---|---|
| $A_1, A_2$ | gas–matrix interface area and matrix–effective medium interface area |
| $A_s$ | arbitrary section of the pore |
| $A_{gj}, B_{gj}, A_{mj}, B_{mj}, A_{ej}, B_{ej}, C$ | real constants |
| $\mathrm{d}A_1, \mathrm{d}A_1^*, \mathrm{d}A_p$ | arbitrary infinitesimal areas |
| $\mathrm{d}F$ | view factor |
| $H, H_0$ | temperature gradient and far-field temperature gradient |
| $k$ | thermal conductivity |
| $\mathbf{n}$ | a normal unit vector |
| $q$ | heat flux |
| $Q_p, Q^r_{As}$ | heat quantity |
| $R$ | radius |
| $T$ | temperature |
| $V$ | volume |
| $\langle \bullet \rangle$ | averaging over the representative volume element |

*Greek*

| | |
|---|---|
| $\lambda$ | porosity |
| $\sigma$ | Stefan-Boltzmann constant |
| $\varepsilon$ | emissivity |
| $\rho$ | reflectivity |

*Subscripts*

| | |
|---|---|
| 1, $g$ | gas in the pore |
| 2, $m$ | matrix |
| $e$ | effective medium |

*Superscripts*

| | |
|---|---|
| $c$ | the contribution of the conduction |
| $r$ | the contribution of the radiation |
| *out* | emission |
| *in* | incidence |

## Acknowledgements

The work was supported by the National Natural Science Foundation of China under Grant NNSFC 10972020, 11061130550 and 11172023, and the Fundamental Research Funds for the Central Universities.

## References

[1] Y.Z. Yang, J.L. Yang, T. Zeng and D.N. Fang, Chin. Q. Mech. 28 (2007) p.503.
[2] S.Y. Zhao, B.M. Zhang and S.Y. Du, Chin. J. Aeronaut. 22 (2009) p.569.
[3] P. Cheng and C.T. Hsu, J. Porous Media 2 (1999) p.19.
[4] Y.C. Chiew and E.D. Glandt, Ind. Eng. Chem. Fund. 22 (1983) p.276.
[5] X.G. Liang and W. Qu, Int. J. Heat Mass Trans. 42 (1999) p.1885.
[6] A.M. Druma, M.K. Alam and C. Druma, Int. J. Therm. Sci. 43 (2004) p.689.
[7] S.T. Liu and Y.C. Zhang, Multidiscip. Model. Mater. Struct. 2 (2006) p.327.
[8] M.R. Wang and N. Pan, Int. J. Heat Mass Trans. 51 (2008) p.1325.
[9] C.Y. Zhao, S.A. Tassou and T.J. Lu, Int. J. Heat Mass Trans. 51 (2008) p.929.
[10] P.S. Liu, Phil. Mag. Lett. 90 (2010) p.447.
[11] E.H. Kerner, Proc. Phys. Soc. B 69 (1956) p.808.
[12] R.M. Christensen and K.H. Lo, J. Mech. Phys. Solid 27 (1979) p.315.
[13] T. Miloh and Y. Benveniste, J. Appl. Phys. 63 (1988) p.789.
[14] R.M. Christensen, J. Mech. Phys. Solid 38 (1990) p.379.
[15] C.P. Jiang and Y.K. Cheung, Int. J. Solid Struct. 35 (1998) p.3977.
[16] C.P. Jiang, Z.H. Tong and Y.K. Cheung, Int. J. Solid Struct. 40 (2003) p.2589.
[17] Y.M. Lee, R.B. Yang and S.S. Gau, Int. Comm. Heat Mass Trans. 33 (2006) p.142.
[18] Z.H. Tong, S.H. Lo, C.P. Jiang and Y.K. Cheung, Int. J. Solid Struct. 45 (2008) p.5205.
[19] C.P. Jiang, F.L. Chen, P. Yan and F. Song, Phil. Mag. 90 (2010) p.3601.
[20] H. Le Quang, Q.-C. He and G. Bonnet, Phil. Mag. 91 (2011) p.3358.
[21] R. Siegel and J.R. Howell, *Thermal Radiation Heat Transfer*, Taylor & Francis, London, 1992.
[22] J. Francl and W.D. Kingery, J. Am. Ceram. Soc. 37 (1954) p.99.
[23] J.S. Agapiou and M.F. DeVries, J. Heat Trans. 111 (1989) p.281.
[24] J.D. McClelland, Materials and structures, physical measurements program, Report No. TDR-930 TR-1, Aerospace Corporation, 1962, p.2240.